J|P|S|T

http://jpst.irost.ir

Journal of

Particle Science and Technology

IROST

Fe₃O₄@SiO₂-SO₃H Nanoparticles: An efficient magnetically retrievable catalyst for esterification reactions

Zeynab Shahedi, Yagoub Mansoori*

Department of Applied Chemistry, Faculty of Science, University of Mohaghegh Ardabili, Ardabil, Iran

HIGHLIGHTS

- A Silica-based magnetic acid catalyst has been prepared.
- Esterification reaction of mono- and dicarboxylic acids by the catalyst has been studied.
- Hammett acidity function has been used for evaluation of the catalyst acidity.

GRAPHICAL ABSTRACT
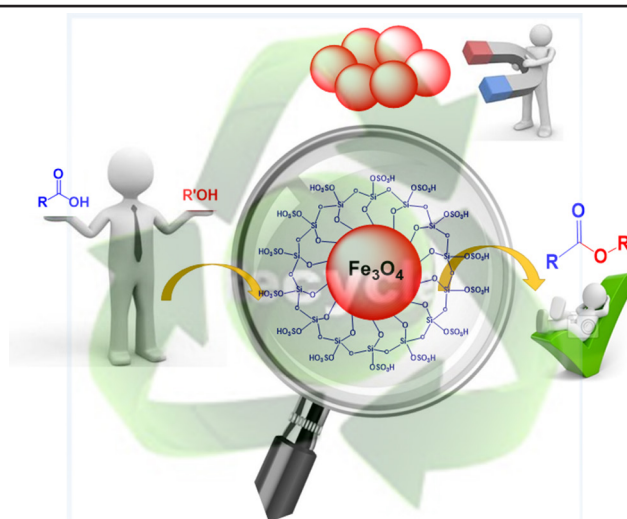
ARTICLE INFO

ABSTRACT

In this study, magnetite nanoparticles were obtained from Fe(II) and Fe(III) salts in an alkaline medium. The nanoparticles were then protected from oxidation by a silica shell formed by the sol-gel method using tetraethoxy orthosilicate (TEOS) in an EtOH/H₂O mixture. The synthesized Fe₃O₄@SiO₂-SO₃H magnetic nanocatalyst was characterized with Fourier transform infrared (FT-IR) spectroscopy, wide angle X-ray diffraction (WXRD), thermal gravimetric analysis (TGA), energy-dispersive X-ray (EDX) spectroscopy, transmission electron microscopy (TEM), vibrating sample magnetometer (VSM), Hammett acidity function and pH analysis as well as Brunauer-Emmett-Teller surface area measurement (S$_{BET}$). Finally, the esterification reaction of phthalic anhydride, mono- and dicarboxylic acids with various alcohols was chosen to show the catalytic activity of the magnetic nanocatalyst. The reaction conditions were optimized and catalyst recovery was also demonstrated. The nanocatalyst was magnetically separated and reused several times without significant loss of activity.

1. Introduction

Organic esters are a highly important group of low molecular weight nonvolatile compounds, which have applications in different areas of the chemical industry such as perfumes, flavors, pharmaceuticals, plasticizers, solvents and intermediates [1]. They are usually obtained through the esterification reaction between corresponding acids/anhydrides and alcohols or trans-esterification reactions in the presence of acidic catalysts. Homogeneous acid catalysts such as sulfuric acid, methane sulfonic acid, p-toluene sulfonic acid, and sodium hydrogen sulfate are the most conventional catalysts used in these reactions. Titanium alkylates and organotin compounds are also used as amphoteric catalysts at elevated temperatures (200 °C) [2]. Corrosion, loss of catalyst, and environment problems coming from acidic wastes are some inevitable characteristics of these catalysts. In recent years, to minimize waste and atom economy in the use of raw materials, traditional homogeneous acid catalysts have been gradually replaced by more eco-friendly, sustainable resources and reusable catalysts. Owing to their potential applications for replacing liquid mineral acids currently used in industry, solid acid catalysts have received significant attention [3]. The recycling of strong solid acids in chemical reactions is compatible with the principles of green chemistry. These catalyzed processes consume the minimum energy and reagents or minimize waste [4]. These catalysts have many advantages including easy separation, minimal corrosion, enhanced product selectivity, high catalytic activity, good recyclability, and simple handling requirements [5-7].

Utilization of various supports, such as silica, carbon, and zirconia, have been reported for homogeneous catalysts/reagents [8-11]. In addition, organic polymers have also been extensively studied for this purpose [12]. In spite of numerous advantages in some cases, these supports retain some of the common drawbacks that pertain to the traditional and difficult isolation procedure after the completion of reactions and most importantly are deficient in terms of reusability.

Recently, magnetite-supported catalysts have been considered as suitable alternatives for existing heterogeneous catalysts. Functionalized magnetic nanoparticles have many advantages such as biocompatibility, easy renew ability and recovery by magnetic separation, thermal stability, large surface area and higher loading of active sites [13]. Magnetite nanoparticles (MNPs) have been noted for their superparamagnetic property, high coercivity and low Curie temperature [3,14-16]. They have found wide applications in magnetic recording, drug delivery, adsorption, catalysis, and separation [17-19]. Easily prepared MNPs are inert, inexpensive, and most importantly they can be separated magnetically and reused multiple times for several reaction cycles. These magnetic nanomaterials can also bind with non-magnetic target molecules through some intermediates forming substrates for various potential applications, they can then be recovered or separated from the solution/complex magnetically [11]. However, they have some drawbacks such as instability in humid air and monotonous surface characteristic. In addition, neat MNPs have found limited applications due to their tendency to make aggregates and strong inter-particle interaction. For this reason, surface coating of MNPs with a suitable material is necessary. The coated layer would be an inert surface (chemical, thermal and mechanical stability) with compatible surface chemistry for their application of specific targeting. Therefore, the development of strategies to coat naked MNPs for stabilization from aggregation over a long period is currently a subject of increasing interest. Functionalized magnetic nanoparticles can be easily separated from products by an external magnet and reused. This kind of separation prevents the loss of solid catalyst in the process and it is not time-consuming. It also enhances product purity and optimizes operational costs [20].

Silica is the most preferred and widely accepted coating among the inorganic materials since the surface chemistry of a silica shell is compatible with various chemicals and biomolecules for bioconjugation [11]. It has been exploited as a coating material for magnetic nanoparticles. It is known that an inert silica shell around the surface of MNPs prevents their aggregation in liquid and improves their chemical stability. The silica layer stabilizes the MNPs in two different ways. First, by shielding the magnetic dipole interaction with the silica shell. And second, the silica nanoparticles are negatively charged, and the coulomb repulsion of the magnetic nanoparticles is enhanced by the silica layer [19].

The use of $Fe_3O_4@SiO_2$-SO_3H as a magnetically retrievable acid catalyst for Knoevenagel condensation and Michael addition reactions [21], synthesis of 1,8-dioxo-octahydroxanthene derivatives [22] and

1-substituted 1*H*-tetrazoles [23], rapid synthesis of amidoalkyl naphthols [24], one-pot solvent-free synthesis of indazolo[2,1-*b*]phthalazine-triones and pyrazolo[1,2-*b*]phthalazine-diones [25], and three-component condensation of indoles, aldehydes and thiols [26] have been studied. Owing to the importance of esterification reactions from an industrial point of view, the present investigation aims to study the catalytic activity of this catalyst in the esterification reaction of mono- and dicarboxylic acids with various alcohols. This work was originally performed with an easier work-up, cleaner reaction, lower cost, and reduction of the amount of acidic waste, which are all extremely important in terms of environmental and economic considerations. The reactions were cleanly carried out in toluene as the solvent and in the presence of Fe_3O_4@SiO_2-SO_3H as the solid magnetic catalyst. Easy reaction conditions, moderate catalytic activity, catalyst recyclability, simple magnetically work-up and lack of acidic waste make Fe_3O_4@SiO_2-SO_3H an effective green catalyst for the esterification reaction. The prepared esters are important compounds and have found wide applications as plasticizers and synthetic ester base lubricants.

2. Experimental

2.1. Instruments

The FTIR (KBr) spectra were recorded on a PerkinElmer RXI spectrophotometer (2 w/w% in KBr, resolution 4 cm^{-1}, scan no. 6). WXRD spectra were recorded at room temperature on a Philips (X-Pro) X-ray diffractometer by using Ni-filtered Cu-Kα radiation. The scanning rate was 1°/min over a 2θ range of 10-80°. Thermogravimetric analyses (TGA) of the samples were carried out on a Linseis STA PT-1000. The TEM analyses were done on a transmission electron microscope (EM10C, Zeiss) with an acceleration voltage of 80 kV. Ultrasonication was performed using a Dr. Heilscher high intensity ultrasound processor UP200H, Germany (13 mm diameter titanium horn, 200 W/cm^2, 23 kHz). Dispersing of the nanoparticles was done in a Parsonic 7500S ultrasonic bath (Pars Nahand Eng. Co., Iran). Magnetization measurements were performed at room temperature using a vibrating sample magnetometer (VSM, 4 inch, Meghnatis Daghigh Kavir Co., Iran) with a maximum magnetic field of 10 kOe. UV-Vis spectra were obtained on a Unico-2100 spectrophotometer. The EDX characterization of the catalyst was performed using a Philips X-30 energy dispersive X-ray spectrometer. The single point N_2 adsorption/desorption analyses according to the BET (Brunauer-Emmett-Teller) method were performed at -196 °C using an automated gas adsorption analyzer (Sibata SA-1100).

2.2. Materials

All solvents were of laboratory grade and dried according to procedures described in the literature [27]. The other chemicals were also of laboratory grade, obtained from Merck Co. and used without further purification.

2.3. Synthesis of MNPs

The synthesis of MNPs was followed by a facile ultrasound assisted method. In a typical procedure, an aqueous solutions of ferric chloride (10 ml, 0.6 M) was added to a ferrous sulfate (10 ml, 0.3 M, in HCl 2 M) solution. The mixture was added dropwise into a 100 ml ammonia solution (0.8 M), while sonicating under argon atmosphere over 30 min. The resulting suspension was cooled down to room temperature and the black precipitate was separated magnetically. The nanoparticles were washed three times with 50 ml portions of ethanol and then dried under vacuum. FT-IR (KBr) ν cm^{-1}: 3406 (br. m), 1630 (w), 586 (s).

2.4. Preparation of nano-Fe_3O_4@SiO_2 core shells

The Fe_3O_4@SiO_2 nanospheres were prepared by a modified Stöber method [23,28]. Briefly, the Fe_3O_4 nanoparticles (0.500 g, 2.16 mmol) were dispersed in a mixture of ethanol (50 ml), deionized water (5 ml) and TEOS (0.20 ml, 0.90 mmol), 5.0 ml of NaOH (10% wt), and then ultrasonicated for 30 min. This mixture was stirred mechanically for 30 min at room temperature. Then, the product was separated by an external magnet and washed with deionized water and ethanol three times and dried at 80 °C for 10 h. FT-IR (KBr) ν cm^{-1}: 3406 (br, s), 1630 (m), 1030 (s), 586 (s).

2.5. Preparation of Fe_3O_4@SiO_2-SO_3H

A suction flask was equipped with a constant pressure

dropping funnel and a gas outlet was evacuated through an adsorbing solution of alkali trap. $Fe_3O_4@SiO_2$ core-shells (1.000 g) were added into the flask and dispersed ultrasonically for 10 min in dry CH_2Cl_2 (50 ml). Chlorosulfonic acid (1.40 ml, 21.03 mmol) was added dropwise to a cooled ice-bath dispersion of $Fe_3O_4@SiO_2$ during 30 min. After the completion of the addition, the mixture was shaken for an hour, while the residual HCl was eliminated by suction. The product was then separated from the reaction mixture by a magnetic field, washed several times with dried CH_2Cl_2 and dried in vacuum. Finally, $Fe_3O_4@SiO_2-SO_3H$ was dried under vacuum at 60 °C [23]. FT-IR (KBr) v cm^{-1}: 3406 (br, s), 1630 (w), 1133 (br,s), 1075 (br, s), 1030 (br, s), 586 (m).

2.6. Esterification of phthalic anhydride (PA), mono-, and dicarboxylic Acids

In a round-bottom flask equipped with an efficient reflux condenser and a Dean-Stark trap, a mixture of carboxylic acid or anhydride, alcohol, and the catalyst was refluxed in toluene for the desired time. The reaction progress was monitored by TLC (petroleum ether/ethyl acetate). After the completion of reaction, the catalyst was separated by an external magnet. The solvent was evaporated under reduced pressure and the residue was dissolved in 5 ml of ethanol. The extent of conversions was calculated by the determination of the acid numbers (mg KOH/g) of the crude reactions mixture using eq. (1) [29].

$$Conversion\ (\%) = [(a_1 - a_2) \times 100]/a_1 \qquad (1)$$

where "a_1" is the acid number of the reaction mixture at the beginning (without catalyst), and "a_2" is the acid number of the crude reaction mixture after the work-up.

3. Results and Discussion

3.1. Preparation of $Fe_3O_4@SiO_2-SO_3H$ nano-catalyst

The co-precipitation method was used to prepare MNPs from the aqueous Fe(II) and Fe(III) solutions. The MNPs were then coated with a silica shell to protect the nanoparticles from oxidation and provided reaction sites for further functionalization. The reaction of $Fe_3O_4@SiO_2$ core-shells with chlorosulfonic acid gave $Fe_3O_4@SiO_2-SO_3H$ nanoparticles, Scheme 1.

## 3.2. Characterization of the $Fe_3O_4@SiO_2-SO_3H$ nanocatalyst

3.2.1. FT-IR Spectral Analysis

The FT-IR spectra of Fe_3O_4, $Fe_3O_4@SiO_2$ and $Fe_3O_4@SiO_2-SO_3H$ are presented in Figure 1a-c. The stretching vibrations related to Fe–O and Si–O–Si bonds appeared at 586 cm^{-1} and 1030 cm^{-1}, respectively. The broad band appearing at 1630 cm^{-1} belongs to the bending vibration of physically adsorbed water molecules. The S=O bond of the sulfonic acid functional group appeared at 1075 cm^{-1}.

3.2.2. WXRD Analysis

The WXRD patterns of Fe_3O_4 and $Fe_3O_4@SiO_2-SO_3H$ are shown in Figure 2a-b. Six characteristic peaks for Fe_3O_4 were observed in both samples. These peaks correspond to (220), (311), (400), (422), (511) and (440) planes of cubic magnetite nanoparticles (JCPDS-ICDD Copyright 1938, file No. 01-1111) with the Fd-3m Space group [30]. The position and the relative intensities of all peaks are consistent with the standard

$$Si(OC_2H_5)_4 + 4H_2O \longrightarrow Si(OH)_4 + 4C_2H_5OH$$
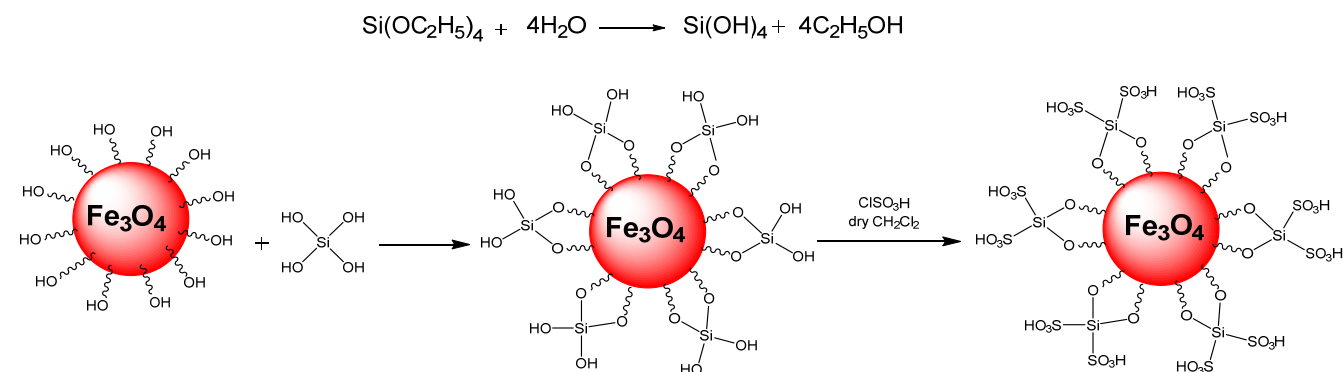
Scheme 1. Preparation of the $Fe_3O_4@SIO_2-SO_3H$ nanocatalyst.
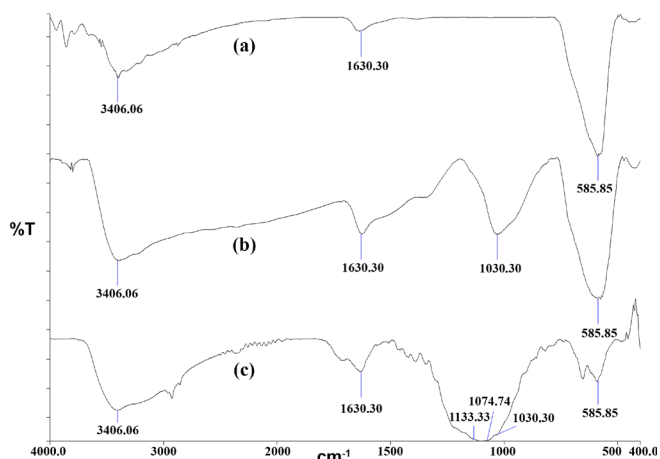
Fig. 1. The comparative FT-IR spectra of (a) nano-Fe_3O_4, (b) $Fe_3O_4@SiO_2$, and (c) $Fe_3O_4@SiO_2$-SO_3H.

Fig. 3. TGA thermograms (N_2 atmosphere, scan rate of 10 ºC/min) of (a) nano-Fe_3O_4, (b)$Fe_3O_4@SiO_2$ and (c) $Fe_3O_4@SiO_2$-SO_3H.

WXRD pattern of Fe_3O_4, confirming retention of the crystalline structure during the functionalization of MNPs. The average crystallite size D can be calculated using the Scherrer equation (2):

$$L = K\lambda / \beta cos\theta \qquad (2)$$

where, L is the coherent length, λ is the wavelength of X-ray radiation (Cu_α=1.54 Å), β is the full width at half maxima (FWHM) of the peak and θ is the Bragg diffraction angle. In the case of spherical crystallite, it is given by L=(3/4)D [31]. The average particle size of Fe_3O_4 was estimated to be approximately 21 nm.

3.2.3. TGA Measurements

The TGA curves of MNPs, $Fe_3O_4@SiO_2$ and $Fe_3O_4@SiO_2$-SO_3H are shown in Figure 3. A gradual mass loss with approximately 2.66% and 5.10% mass is observed for the MNPs and $Fe_3O_4@SiO_2$ from ambient temperature to 600 °C (Figure 3-a,b), respectively. This

molecules (below 100 °C) and surface de-hydroxylation in the range of 200-600 °C. A similar behavior is also observed by a mass loss of approximately 1.10% in the TGA curve of $Fe_3O_4@SiO_2$-SO_3H (Figure 3-c). In addition, a two-stage decomposition process is seen corresponding to different mass loss ranges. In the first region, a mass loss of approximately 10.85% occurred between 100 °C and 330 °C which is related to the removal of −SO_3H groups. Finally, a mass loss of approximately 5.66% occurred between 330 °C and 600 °C and was related to the sudden mass loss in the sulfonic acid groups [32]. The TGA thermogram of $Fe_3O_4@SiO_2$-SO_3H reveals that the prepared nanocatalyst could be used in organic reactions due to high thermal stability (up to 150 °C). TGA measurement can also be used to calculate the amount of sulfonic acid loading [33]. The difference between mass losses of $Fe_3O_4@SiO_2$ and $Fe_3O_4@SiO_2$-SO_3H after heating at 600 ºC (Δm=11.96%) can be attributed to the multitude of surface sulfonic acid groups (119.6 mg/g of nanoparticles) using eq. (3).

$$Sulfonic\ acid\ loading\ (mg/g) = (\Delta m/100) \times 1000 \qquad (3)$$

3.2.4. TEM and EDX analysis

The TEM images of MNPs and $Fe_3O_4@SiO_2$-SO_3H nanoparticles are shown in Figure 4. As observed, MNPs exhibit uniform spherical morphology with a particle size of approximately 15-20 nm, Figure 4-a. This value falls in the size range of superparamagnetic MNPs which are strongly recommended for in vivo biomedical applications [33,34]. The presence of the sulfonic acid functionalized silica shell around the


Fig. 2. XRD patterns of (a) Fe_3O_4, and (b) $Fe_3O_4@SiO_2$-SO_3H nanoparticles.

(a)

(b)
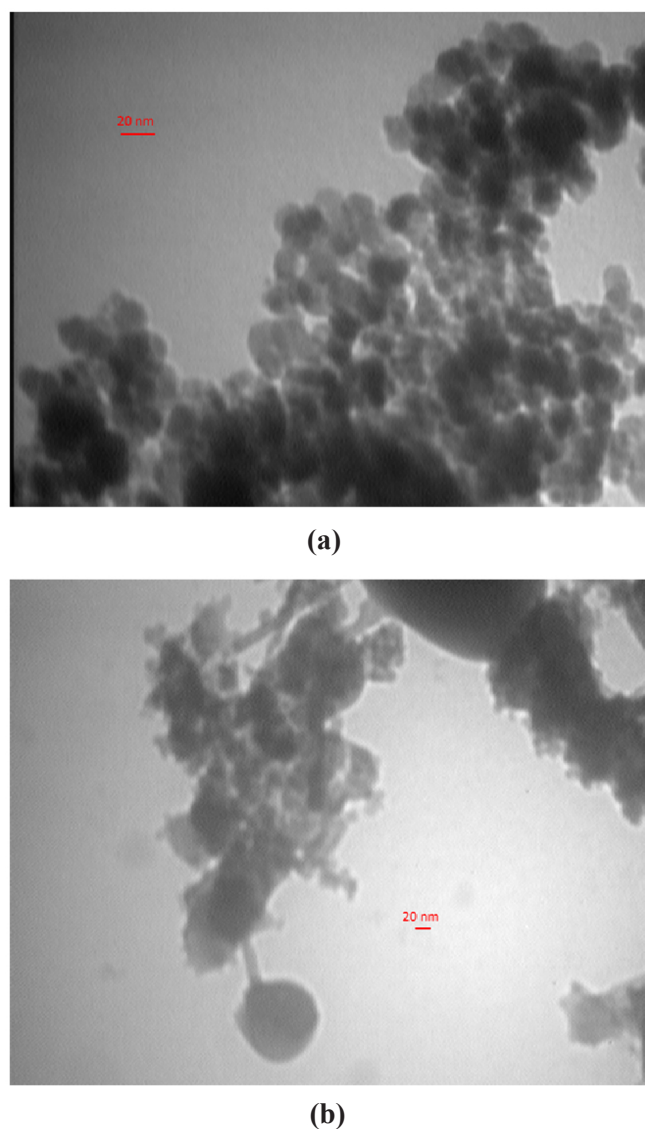
Fig. 4. The TEM images of (a) Fe_3O_4, and (b) $Fe_3O_4@SiO_2-SO_3H$.

MNPs can be distinguished in Figure 4-b. The formation of silica shell and subsequent functionalization were further confirmed by X-ray analysis (EDX) of the obtained nanocatalyst, Figure 5. This analysis revealed the existence of Fe, Si, S, and O elements.
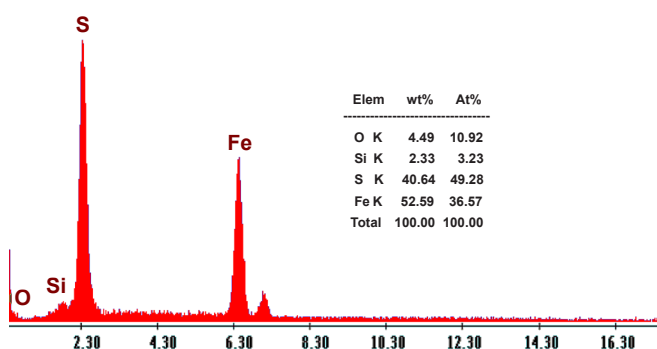

Fig. 5. EDX spectrum of $Fe_3O_4@SiO_2-SO_3H$.

3.2.5. Magnetization and surface area measurements

The magnetic moments of the prepared nanoparticles were measured over a range of applied fields between 8500 and -8500 Oe at 298 K. The magnetization curves are shown in Figure 6 and the results are summarized in Table 1. The naked Fe_3O_4, $Fe_3O_4@SiO_2$ core-shells and $Fe_3O_4@SiO_2-SO_3H$ have the saturation magnetization values of 61.4, 58.1 and 9.0 emu/g, respectively. The saturation magnetization values are below the values reported for bulk magnetite particles (M_s= 92-100 emu/g). The high magnetization endows the microspheres with fast responsivity during magnetic separation. This may be attributed to the fact that below a critical size MNPs may exist as a single domain and show the unique phenomenon of superparamagnetism [5,35]. These saturation magnetization values clearly indicate decreasing magnetization after coating of Fe_3O_4 with SiO_2 and then sulfonic acid loading. This could be attributed to the formation of two non-magnetic coating layers of SiO_2 and sulfonic acids in the core-shell structure. The small field coercivity of $Fe_3O_4@SiO_2-SO_3H$ (H_c= 12.0 Oe) demonstrates that the prepared catalyst has superparamagnetic characteristics with a remanence magnetization of M_r= 0.3 emu/g and remanence ratio of M_r/M_s= 0.03.

As the external magnetic field was applied, the nanoparticles of the catalyst were attracted towards the magnet leaving the toluene solution clear and transparent. The catalyst redispersed quickly with a slight shake when the magnetic field was removed. This shows that the catalyst possess excellent magnetic responsivity and redispersibility, which is an advantage for its applications. Ferromagnetic nanoparticles usually suffer from aggregation upon redispersion, whereas the redispersion of the superparamagnetic nanoparticles in solution occurs without severe aggregation.

The adsorption characteristics of a material are related to its physical morphology. Therefore, the

Table 1. Magnetic properties of MNPs, $Fe_3O_4@SiO_2$ and $Fe_3O_4@SiO_2-SO_3H$.

Sample	M_s (emu/g)[a]	M_r (emu/g)[b]	H_c (Oe)[c]	M_r/M_s[d]
Fe_3O_4	61.4	3.2	31.0	0.05
$Fe_3O_4@SiO_2$	58.1	0.5	5.0	0.01
$Fe_3O_4@SiO_2-SO_3H$	9.0	0.3	12.0	0.03

[a]Saturation magnetization; [b]Remanent magnetization; [c]coercive force; [d]Remanence ratio.
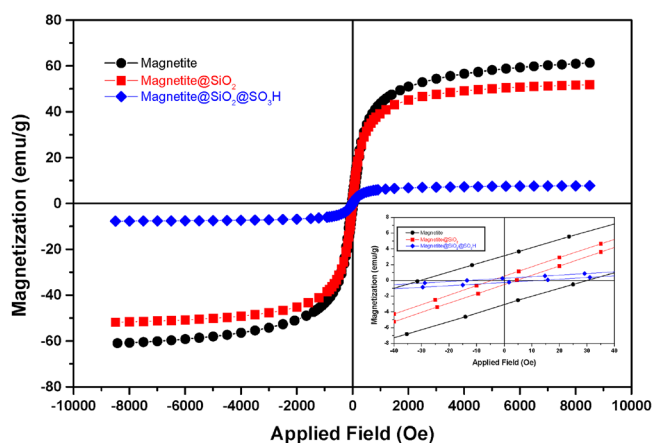
Fig. 6. Magnetization curves for the MNPs, $Fe_3O_4@SiO_2$ and $Fe_3O_4@SiO_2$-SO_3H at room temperature.

surface morphology of the prepared nanoparticles is an important factor affecting its performance. The specific surface area (S_{BET}) of $Fe_3O_4@SiO_2$ and $Fe_3O_4@SiO_2$-SO_3H was measured according to the BET (Brunauer-Emmett-Teller) method. As observed in Table 2, the specific surface area of the nanocatalyst is lower than that of $Fe_3O_4@SiO_2$ nanoparticles. The main reason for the smaller SBET of the decorated catalyst, as compared with the support, is the anchoring of the sulfur species which blocked the pores.

3.2.6. Acidity of $Fe_3O_4@SiO_2$-SO_3H nanocatalyst

The acidity strength of an acid in organic solvents can be effectively expressed by the Hammett acidity function (H_0) [36]. This can be calculated using eq. (4).

$$H_0 = pK(I)_{aq} + log([I]_s/[IH^+]_s) \qquad (4)$$

where, $[I]_s$ and $[IH^+]_s$ are the molar concentrations of the un-protonated and protonated forms of the indicator base (p-nitroanilines, $pK(I)_{aq}= 0.99$), respectively. According to the Beer-Lambert Law, $[I]_s$ and $[IH^+]_s$ can be calculated using the UV-visible spectrum. In the present experiment, CCl_4 was chosen as the solvent due to its aprotic nature. The λ_{max} of the un-protonated form of the indicator was observed at 330 nm in CCl_4. As

shown in Figure 7, the absorbance of the un-protonated form in the presence of $Fe_3O_4@SiO_2$-SO_3H was weak when compared to the sample of the indicator in CCl_4, which reveals that the indicator was partially protonated. The results showing the acidity strength of the catalyst are summarized in Table 3. As observed, the Hammett acidity function of $Fe_3O_4@SiO_2$-SO_3H (H_0 =1.06) also approves the synthesis of the acid catalyst with a good density of acid sites (–SO_3H groups) on the surface.

The loaded sulfonic acid was calculated from the pH analysis of the proton-exchanged brine solutions [25]. For an aqueous solution of NaCl (1.0 M, 25 ml) with an initial pH of 5.90, nanocatalyst (0.100 g) was added and stirred for 24 h. at room temperature. The pH of the solution was measured (pH = 1.84) after removing the catalyst with an external magnet. This is equal to a loading of 3.61 mmol $SO_3H.g^{-1}$ of acidic catalyst. These results in conjunction with the Hammett acidity function (H_0) confirm the synthesis of a new catalyst with a good density of acid sites (−SO_3H groups) on the surface.

3.3. Esterification of phthalic anhydride, mono- and dicarboxylic Acids

In order to optimize the amount of catalyst, a 1:2 molar mixture of phthalic anhydride and n-butanol was refluxed in toluene for 10 h with different quantities of
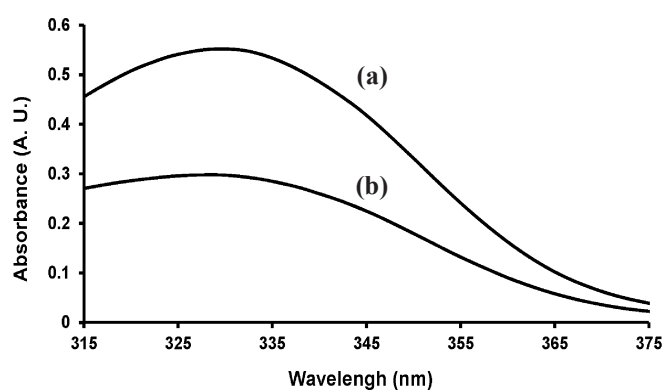

Fig. 7. Absorption spectra of (a) 4-nitroaniline (indicator) and (b) $Fe_3O_4@SiO_2$-SO_3H (catalyst) in CCl_4.

Table 2. Measured S_{BET} of $Fe_3O_4@SiO_2$ and $Fe_3O_4@SiO_2$-SO_3H.

Sample	S_{BET} (m²/g)
$Fe_3O_4@SiO_2$	173.7
$Fe_3O_4@SiO_2$-SO_3H	162.3

Table 3. Calculation of Hammett acidity function (H_0) of $Fe_3O_4@SiO_2$-SO_3H.*

Entry	Catalyst	A_{max}	$[I]_s$ (%)	$[IH^+]_s$ (%)	H_0
1	Blank	0.5518	100.0	0.0	-
2	$Fe_3O_4@SiO_2$-SO_3H	0.2979	54.0	46.0	1.06

* Conditions for UV-visible spectrum measurement: solvent, CCl_4; indicator, 4-nitroaniline ($pK(I)_{aq} = 0.99$), 3×10^{-5} mol.L^{-1}; catalyst (10 mg), 25 °C.

the catalyst, Scheme 1. A Dean-Stark trap was used for water removal and the reaction progress was followed by TLC (petroleum ether:ethyl acetate; 85:15). The results are listed in Table 4.
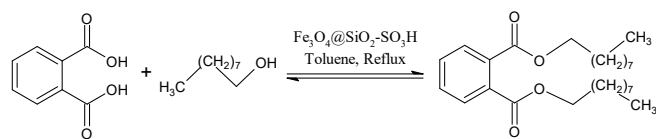
Scheme 2. Esterification of PA by *n*-nonanol in the presence of $Fe_3O_4@SiO_2\text{-}SO_3H$.

As observed, the reaction does not proceed in the absence of the catalyst (Entry 1), and with 5 wt% of the total weight of PA and *n*-butanol the conversion reaches maximum in 10 h. Therefore, it was chosen as the optimum amount of the catalyst for the other esterification reactions. The good catalytic activity of $Fe_3O_4@SiO_2\text{-}SO_3H$ relates to the presence of sulfonic acid groups on the surface, which provide efficient acidic sites. Then, the capability of the nanocatalyst toward the esterification of PA (Table 5), monocarboxylic acids (Table 6), and dicarboxylic acids (Table 7) by different alcohols was studied. The results obtained for esterification of mono- and dicarboxylic acids were compared with the results obtained by $Fe_3O_4@ZrO_2\text{-}SO_3H$ reported earlier [37]. As can be seen, in all cases, the conversion obtained by the catalyst in this study are higher than those conversion obtained by $Fe_3O_4@ZrO_2\text{-}SO_3H$. This can be attributed to a higher acidity strength of $Fe_3O_4@SiO_2\text{-}SO_3H$ ($H_0=1.06$) than that of $Fe_3O_4@ZrO_2\text{-}SO_3H$ ($H_0=1.47$). Most of the prepared compounds are industrially valuable as plasticizers and synthetic ester base lubricants. The FT-IR spectra of the prepared esters and diesters are in accordance with the spectra reported in the Spectral Database for Organic

Compounds (SDBS) and the literature reported values. We could not correlate the extent of conversion with the structures of alcohols and carboxylic acids. As a major trend, higher alcohols have better reaction yields, and the extent of conversion is also better in long alkyl chain dicarboxylic acids (adipic acid and sebacic acid, Table 7, Entries 4-9) than that of monocarboxylic acids. This is a positive point, since the diesters of long chain dicarboxylic acids can be considered as excellent base lubricants due to good properties at high and low temperatures, excellent viscosity vs. temperature relationship, low volatility, lubricity, additive solubility, frictional properties, and biodegradability [6,38]. Ethyl esters were obtained in low yields even with the excess amount of ethanol (ethanol used in and as solvent) due to the low reaction temperature and volatility of EtOH. A possible mechanism for the esterification reaction catalyzed by $Fe_3O_4@SiO_2\text{-}SO_3H$ can be proposed as Scheme 3.

3.4. Recyclability of the nano-catalyst

Recycling of the catalyst was also examined to determine practical applications of the synthesized magnetic nano-catalyst. For this purpose, the reaction of PA and n-hexanol in the presence of $Fe_3O_4@SiO_2\text{-}SO_3H$ was studied. In this procedure, after the completion of the reaction, the catalyst was separated from the product magnetically and the conversion was calculated after work-up. The catalyst was washed with hot and dry acetone to remove residual product, dried, and then reused in a subsequent reaction. The extent of

Table 4. Optimization of catalyst amount for the esterification of PA by *n*-nonanol.[a]

| Entry	Catalyst weight (wt%)[b]	Conversion (%)[c]
1	0	0
2	2	20
3	3	40
4	5	97
5	7	98

[a] Reaction conditions: PA (0.5 mmol, 0.74 g), *n*-butanol (1 mmol, 0.9 ml), *p*-toluene (30 ml), reflux for 10 h. [b] Based on total weight of PA and *n*-butanol. [c] Calculated based on acid number measurements.
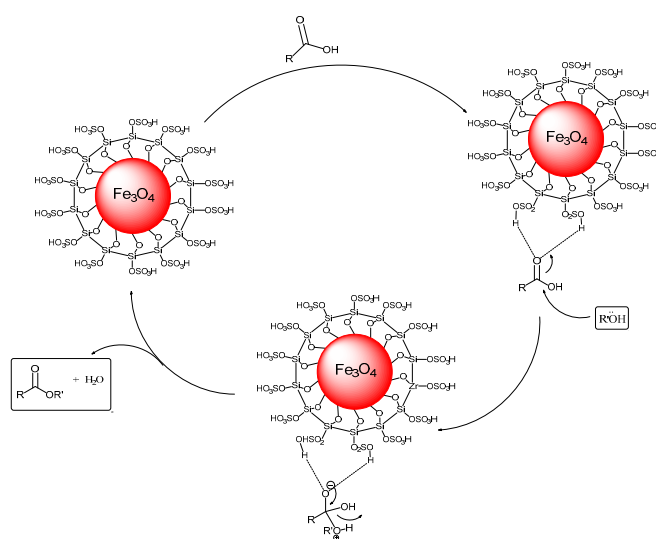
Scheme 3. Proposed reaction pathway for esterification in the presence of $Fe_3O_4@SiO_2\text{-}SO_3H$.

Table 5. Reaction conditions and conversions of PA by various alcohols
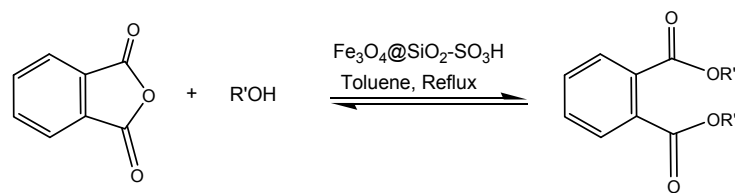
Entry	Alcohol	PA/alcohol molar ratio	Reaction Time (h)	Conversion (%)
1 [a]		EtOH solvent	14	8
2		1:3	12	71
3		1:3	8	97
4		1:1	12	65
5		1:2	12	89
6		1:3	13	86
7		1:3	14	77
8		1:3	13	85
9		1:2	14	40
10		1:3	12	40
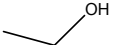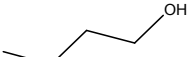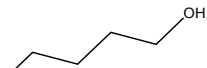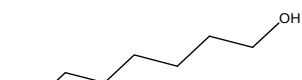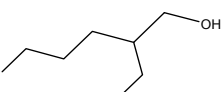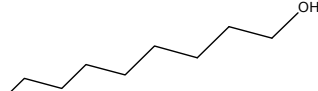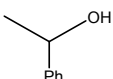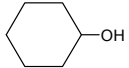
[a] The amount of catalyst was 5 wt% of total weight of phthalic anhydride and alcohol.

conversion did not dropped significantly after re-using of the catalyst five times. This means that the nature of the nano-catalyst is only slightly changed after each run and -SO$_3$H moieties were tightly anchored with the nano-catalyst. The average extent of the conversion after five consecutive runs was 73.4%, which clearly demonstrates the practical recyclability of the catalyst (Figure 8).

4. Conclusion

The esterification reaction of PA, mono- and dicarboxylic acids in the presence of a Fe$_3$O$_4$@SiO$_2$-
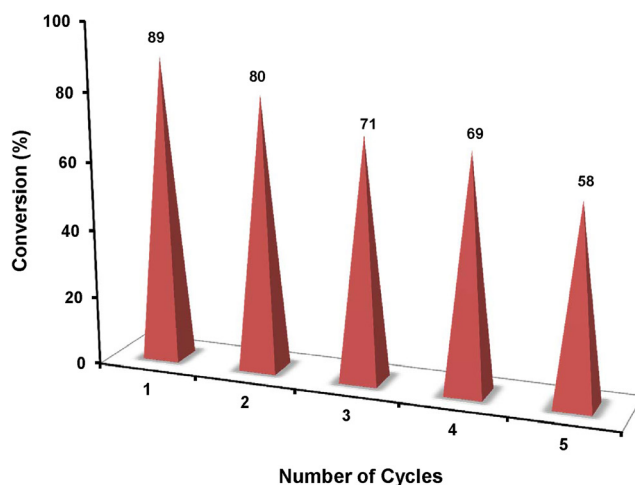
Fig. 8. Recyclability of Fe$_3$O$_4$@SiO$_2$-SO$_3$H.

Table 6. Reaction conditions and conversions of mono-carboxylic acids esterification by various alcohols.

Entry	RCOOH	R′OH	Acid/alcohol molar ratio	Reaction Time (h)	Conversion (%)[a]
1 [b]			EtOH solvent	12	15 (0)
2			1:1	12	30 (10)
3			1:3	12	60 (15)
4			1:1	12	25 (10)
5			1:1	12	25 (16)
6			1:1	14	40 (61)
7			1:1	14	40 (25)
8			1:3	12	85 (50)
9			1:3	12	88 (0)
10			1:2	13	60 (57)
11			1:2	14	71 (44)
12			1:2	12	70 (62)
13 [a]			EtOH solvent	12	15 (20)
14			1:2	12	64 (33)

[a] The values in parenthesis are the conversions obtained by $Fe_3O_4@SiO_2$-SO_3H under the same conditions [38]. [b] The amount of catalyst was 5 wt% of total weight of carboxylic acid and alcohol.

SO_3H nano-catalyst has been studied. In summary, we showed that the prepared catalyst is an efficient heterogeneous magnetic catalyst for this purpose. The use of this catalyst makes industrial processes easier, cleaner, and less complicated. The catalyst can be readily separated from the reaction mixture magnetically and re-used several times without any significant loss of activity. The clean reaction conditions and utilizing a

Table 7. Reaction conditions and conversions of dicarboxylic acids esterification by various alcohols.[a]

Entry	dicarboxylic Acid	Alcohol	Diacid/alcohol molar ratio	Reaction Time (h)	Conversion (%)[a]
1 [b]			EtOH solvent	14	2 (25)
2			1:3	12	88 (75)
3			1:2	12	76 (60)
4			1:3	12	90 (80)
5			1:2	12	82 (76)
6			1:3	12	89 (80)
7			1:2	12	85 (82)
8			1:2	12	80 (75)
9			1:2	13	88 (76)

[a] The values in parenthesis are the conversions obtained by Fe_3O_4@SiO_2-SO_3H under the same conditions [38]. [b] The amount of catalyst was 5 wt% of total weight of dicarboxylic acid and alcohol.

green and magnetically separable heterogeneous catalyst are the main advantages of this catalyst.

Acknowledgement

References

[1] S. Ajaikumar, A. Pandurangan, Esterification of alkyl acids with alkanols over MCM-41 molecular sieves: Influence of hydrophobic surface on condensation reaction, J. Mol. Catal. A-Chem. 266 (2007) 1-10.

[2] A. Ross, Industrial Applications of Organotin Compounds, Ann. N.Y. Acad. Sci. 125 (1965) 107-123.

[3] A. Mobaraki, B. Movassagh, B. Karimi, Magnetic solid sulfonic acid decorated with hydrophobic regulators: A combinatorial and magnetically separable catalyst for the synthesis of α-aminonitriles, ACS Comb. Sci. 16 (2014) 352-358.

[4] S. Rostamnia, A. Nuri, H. Xin, A. Pourjavadi, S.H. Hosseini, Water dispersed magnetic nanoparticles (H₂O-DMNPs) of γ-Fe₂O₃ for multicomponent coupling reactions: a green, single-pot technique for the synthesis of tetrahydro-4H-chromenes and

hexahydroquinoline carboxylates, Tetrahedron Lett. 54 (2013) 3344-3347.

[5] Y. Li, T. Leng, H. Lin, C. Deng, X. Xu, N. Yao, P. Yang, X. Zhang, Preparation of $Fe_3O_4@ZrO_2$ core-shell microspheres as affinity probes for selective enrichment and direct determination of phosphopeptides using matrix-assisted laser desorption ionization mass spectrometry, J. Proteome Res. 6 (2007) 4498-4510.

[6] Y. Mansoori, F.S. Tataroglu, M. Sadaghian, Esterification of carboxylic acids by tributyl borate under solvent- and catalyst-free conditions, Green Chem. 7 (2005) 870-873.

[7] Y. Mansoori, F. Tataroglu Seyidov, S. Bohlooli, M.R. Zamanloo, G.H. Imanzadeh, Esterification of carboxylic acids and diacids by trialkyl borate under solvent- and catalyst-free conditions, Chinese J. Chem. 25 (2007) 1878-1882.

[8] M. A. Zolfigol, Silica sulfuric acid/$NaNO_2$ as a novel heterogeneous system for production of thionitrites and disulfides under mild conditions, Tetrahedron, 57 (2001) 9509-9511.

[9] S.T. Firdovsi, M. Yagoub, A.E. Parvin, Transesterification reaction of dimethyl terephthalate by 2-ethylhexanol in the presence of heterogeneous catalysts under solvent-free condition, Chinese J. Chem. 25 (2007) 246-249.

[10] K. Saravanan, B. Tyagi, H.C. Bajaj, Sulfated zirconia: an efficient solid acid catalyst for esterification of myristic acid with short chain alcohols, Catal. Sci. Technol. 2 (2012) 2512-2520.

[11] A.P. Kumar, J.H. Kim, T.D. Thanh, Y.-I. Lee, Chiral zirconia magnetic microspheres as a new recyclable selector for the discrimination of racemic drugs, J. Mater. Chem. B, 1 (2013) 4909-4915.

[12] N.E. Leadbeater, M. Marco, Preparation of polymer-supported ligands and metal complexes for use in catalysis, Chem. Rev. 102 (2002) 3217-3274.

[13] A. Mobaraki, B. Movassagh, B. Karimi, Hydrophobicity-enhanced magnetic solid sulfonic acid: A simple approach to improve the mass transfer of reaction partners on the surface of the heterogeneous catalyst in water-generating reactions, Appl. Catal. A, 472 (2014) 123-133.

[14] C. Gómez-Polo, A. Gil, S.A. Korili, J.I. Pérez-Landázabal, V. Recarte, R. Trujillano, M.A. Vicente, Effect of the metal support interactions on the physicochemical and magnetic properties of Ni catalysts, J. Magn. Magn. Mater. 316 (2007) e783-e786.

[15] M.B. Gawande, A.K. Rathi, I.D. Nogueira, R.S. Varma, P.S. Branco, Magnetite-supported sulfonic acid: a retrievable nanocatalyst for the Ritter reaction and multicomponent reactions, Green Chem. 15 (2013) 1895-1899.

[16] Z. Wang, D. Wu, G. Wu, N. Yang, A. Wu, Modifying Fe_3O_4 microspheres with rhodamine hydrazide for selective detection and removal of Hg^{2+} ion in water, J. Hazard. Mater. 244-245 (2013) 621-627.

[17] I. Chourpa, L. Douziech-Eyrolles, L. Ngaboni-Okassa, J.-F. Fouquenet, S. Cohen-Jonathan, M. Souce, H. Marchais, P. Dubois, Molecular composition of iron oxide nanoparticles, precursors for magnetic drug targeting, as characterized by confocal Raman microspectroscopy, Analyst, 130 (2005) 1395-1403.

[18] M. Shokouhimehr, Y. Piao, J. Kim, Y. Jang, T. Hyeon, A magnetically recyclable nanocomposite catalyst for olefin epoxidation, Angew. Chem. Int. Edit. 46 (2007) 7039-7043.

[19] S. Laurent, D. Forge, M. Port, A. Roch, C. Robic, L. Vander Elst, R.N. Muller, Magnetic iron oxide nanoparticles: Synthesis, stabilization, vectorization, physicochemical characterizations, and biological applications, Chem. Rev. 108 (2008) 2064-2110.

[20] V.V. Costa, M.J. Jacinto, L.M. Rossi, R. Landers, E.V. Gusevskaya, Aerobic oxidation of monoterpenic alcohols catalyzed by ruthenium hydroxide supported on silica-coated magnetic nanoparticles, J. Catal. 282 (2011) 209-214.

[21] F. Nemati, M.M. Heravi, R. Saeedi Rad, Nano-Fe_3O_4 encapsulated-silica particles bearing sulfonic acid goups as a magnetically separable catalyst for highly efficient Knoevenagel condensation and Michael addition reactions of aromatic aldehydes with 1,3-cyclic diketones, Chinese J. Catal. 33 (2012) 1825-1831.

[22] H. Naeimi, Z. Nazifi, A highly efficient nano-Fe_3O_4 encapsulated-silica particles bearing sulfonic acid groups as a solid acid catalyst for synthesis of 1,8-dioxo-octahydroxanthene derivatives, J. Nanopart. Res. 15 (2013) 1-11.

[23] H. Naeimi, S. Mohamadabadi, Sulfonic acid-functionalized silica-coated magnetic nanoparticles as an efficient reusable catalyst for the synthesis

of 1-substituted 1H-tetrazoles under solvent-free conditions, Dalton T. 43 (2014) 12967-12973.

[24] J. Safari, Z. Zarnegar, A magnetic nanoparticle-supported sulfuric acid as a highly efficient and reusable catalyst for rapid synthesis of amidoalkyl naphthols, J. Mol. Catal. A-Chem. 379 (2013) 269-276.

[25] A.R. Kiasat, J. Davarpanah, Fe_3O_4@silica sulfuric acid nanoparticles: An efficient reusable nanomagnetic catalyst as potent solid acid for one-pot solvent-free synthesis of indazolo[2,1-b]phthalazine-triones and pyrazolo[1,2-b]phthalazine-diones, J. Mol. Catal. A-Chem. 373 (2013) 46-54.

[26] A. Khorshidi, S. Shariati, Sulfuric acid functionalized MCM-41 coated on magnetite nanoparticles as a recyclable core-shell solid acid catalyst for three-component condensation of indoles, aldehydes and thiols, RSC Adv. 4 (2014) 41469-41475.

[27] W.L.F. Armarego, C.L.L. Chai, Purification of laboratory chemicals, 6th ed., Butterworth-Heinemann, Elsevier Inc., Burlington, 2009.

[28] W. Stöber, A. Fink, E. Bohn, Controlled growth of monodisperse silica spheres in the micron size range, J. Colloid Interf. Sci. 26 (1968) 62-69.

[29] F.T. Sejidov, Y. Mansoori, N. Goodarzi, Esterification reaction using solid heterogeneous acid catalysts under solvent-less condition, J. Mol. Catal. A-Chem. 240 (2005) 186-190.

[30] J.D. Hanawalt, H.W. Rinn, L.K. Frevel, Chemical analysis by x-ray diffraction, Ind. Eng. Chem. Res. 10 (1938) 457-512.

[31] A. Guinier, X-ray diffraction: in crystals, imperfect crystals, and amorphous bodies. Courier Dover Publications, New York, 2013.

[32] A. Amoozadeh, S. Rahmani, M. Bitaraf, F.B. Abadi, E. Tabrizian, Nano-zirconia as an excellent nano support for immobilization of sulfonic acid: a new, efficient and highly recyclable heterogeneous solid acid nanocatalyst for multicomponent reactions, New J. Chem. 40 (2016) 770-780.

[33] H. Cao, J. He, L. Deng, X. Gao, Fabrication of cyclodextrin-functionalized superparamagnetic Fe_3O_4/amino-silane core–shell nanoparticles via layer-by-layer method, Appl. Surf. Sci. 255 (2009) 7974-7980.

[34] M. Pooresmaeil, Y. Mansoori, M. Mirzaeinejad, A.L.I. Khodayari, Efficient removal of methylene blue by novel magnetic hydrogel nanocomposites of poly(acrylic acid), Adv. Polym. Tech. 37 (2016) 262-274.

[35] J. Choubey, A.K. Bajpai, Investigation on magnetically controlled delivery of doxorubicin from superparamagnetic nanocarriers of gelatin crosslinked with genipin, J. Mater. Sci.-Mater. M. 21 (2010) 1573-1586.

[36] H. Xing, T. Wang, Z. Zhou, Y. Dai, The sulfonic acid-functionalized ionic liquids with pyridinium cations: Acidities and their acidity-catalytic activity relationships, J. Mol. Catal. A-Chem. 264 (2007) 53-59.

[37] P. Tayeb Oskoie, Y. Mansoori, Fe_3O_4@ZrO_2-SO_3H Nanoparticles: A new magnetically retrievable catalyst for esterification of mono- and dicarboxylic acids, J. Part. Sci. Technol. 4 (2018) 1-12.

[38] G. Van der Waal, Ester base fluids, Unichem International, Gouda, The Netherlands, 1995.